Molecular Therapy
Nucleic Acids
Original Article

The miR-93-3p/ZFP36L1/ZFX axis regulates keratinocyte proliferation and migration during skin wound healing

Xiao Feng,[1,4] Shuangbai Zhou,[2,4] Weilin Cai,[3] and Jincai Guo[1]

[1]Department of Plastic Surgery, Zhejiang Provincial People's Hospital, Hangzhou, China; [2]Department of Plastic and Reconstructive Surgery, Shanghai Ninth People's Hospital, Shanghai Jiao Tong University, Shanghai, China; [3]Department of Dermatologic Surgery, Hangzhou Third People's Hospital, Hangzhou, China

Keratinocyte proliferation and migration are crucial steps during skin wound healing. The functional role of microRNAs (miRs) remains relatively unknown during this process. miR-93 levels have been reported to increase within 24 h of skin wound healing; however, whether miR-93-3p or miR-93-5p plays a specific role in wound healing is yet to be studied. In this study, with the use of an *in vivo* mouse skin wound-healing model, we demonstrate that miR-93-3p is significantly upregulated, whereas there is no change in the expression of miR-93-5p during skin wound healing. In HaCaT cells, miR-93-3p overexpression increased proliferation and migration of the cells, whereas miR-93-3p inhibition had the reverse effect. Additionally, it was evident that ZFP36L1 was a direct target of miR-93-3p in keratinocytes. Further, ZFP36L1 silencing mirrored the consequences observed during miR-93-3p overexpression on both proliferation and migration of keratinocytes. In addition, we demonstrate that zinc-finger X-linked (ZFX), as a target for ZFP36L1, is involved in the promotion of the miR-93-3p/ZFP36L1 axis in keratinocyte proliferation and migration. Ultimately, we found that mouse skin wound model treatment with anti-miR-93-3p delayed wound healing. Overall, our results show that miR-93-3p is a crucial regulator of skin wound healing that facilitates keratinocyte proliferation and migration through ZFP36L1/ZFX axis.

INTRODUCTION

Physiological process, such as wound healing, comprises a number of coordinated molecular and biological events that allow maintenance of skin integrity.[1] Wound-healing classical model categorizes the different events as four concurrent but overlapping phases that include initial hemostasis (up to several hours after injury), followed by inflammation (1–3 days after injury), and this leads to increased proliferation (4–21 days after injury) and finally, tissue remodeling (21 days—1 year) after injury.[2] A crucial stage during the wound-healing process is re-epithelialization, which is regulated by molecular factors and growth factors, such as extracellular matrix (ECM),[3] integrins, matrix metalloproteinases (MMPs), growth factors, and cytokines,[4–9] whereas keratinocyte proliferation and migration are fundamentally important steps in this process. The exploration of the proliferation and migration mechanisms of keratinocytes will help find new targets for promoting wound healing.

MicroRNAs (miRs; miRNAs) represent a class of 22 nucleotide-long non-coding RNA that either represses or degrades mRNA by binding to the 3′ untranslated region (UTR) of the target mRNA.[10] Previously, studies have reported that miRNAs are widely associated with many biological processes; however, recently, they have been identified to regulate keratinocyte proliferation and migration.[11,12] For example, miR-31 has been found to take part in wound healing via regulation of epithelial membrane protein-1.[11,12] miR-203 exerts a specific role in injured skin by controlling the expression of target proteins that are responsible for both keratinocyte proliferation and migration.[13] miR-96-5p was shown to take part in regulation of wound healing by interacting with the BNIP3/FAK pathway.[14] A study identified that the levels of miR-93 have been reported to increase within 24 h of human skin wound-healing initiation.[11] As we all know, miR-93-5p but not miR-93-3p is the abundant product of miR-93. However, whether miR-93-3p or miR-93-5p plays a specific role in wound healing has not yet been studied. Therefore, in this study, we first examined the expression of miR-93-3p and miR-93-5p in the wound edge tissue at indicated time points. Our results showed that miR-93-3p was significantly upregulated, whereas there is no change in the expression of miR-93-5p during mice skin wound healing. Hence, in this study, our focus is to elucidate the roles of miR-93-3p in skin wound healing. We identified that miR-93-3p increases keratinocyte proliferation and migration through the suppression of its downstream target gene, ZFP36L1 (an RNA-binding protein [RBP]). We also identified that zinc-finger X-linked (ZFX), a target of ZFP36L1, promotes keratinocytes cell proliferation and migration. Collectively, results from our study indicate that miR-93-3p plays a vital role in skin wound healing by accelerating keratinocyte proliferation and migration through the regulation of the ZFP36L1/ZFX axis.

Received 14 June 2020; accepted 17 November 2020;
https://doi.org/10.1016/j.omtn.2020.11.017.

[4]These authors contributed equally

Correspondence: Jincai Guo, Department of Plastic Surgery, Zhejiang Provincial People's Hospital, No. 158 Sheng Tang Road, Hangzhou 310000, China.
E-mail: guojincaiketi@163.com

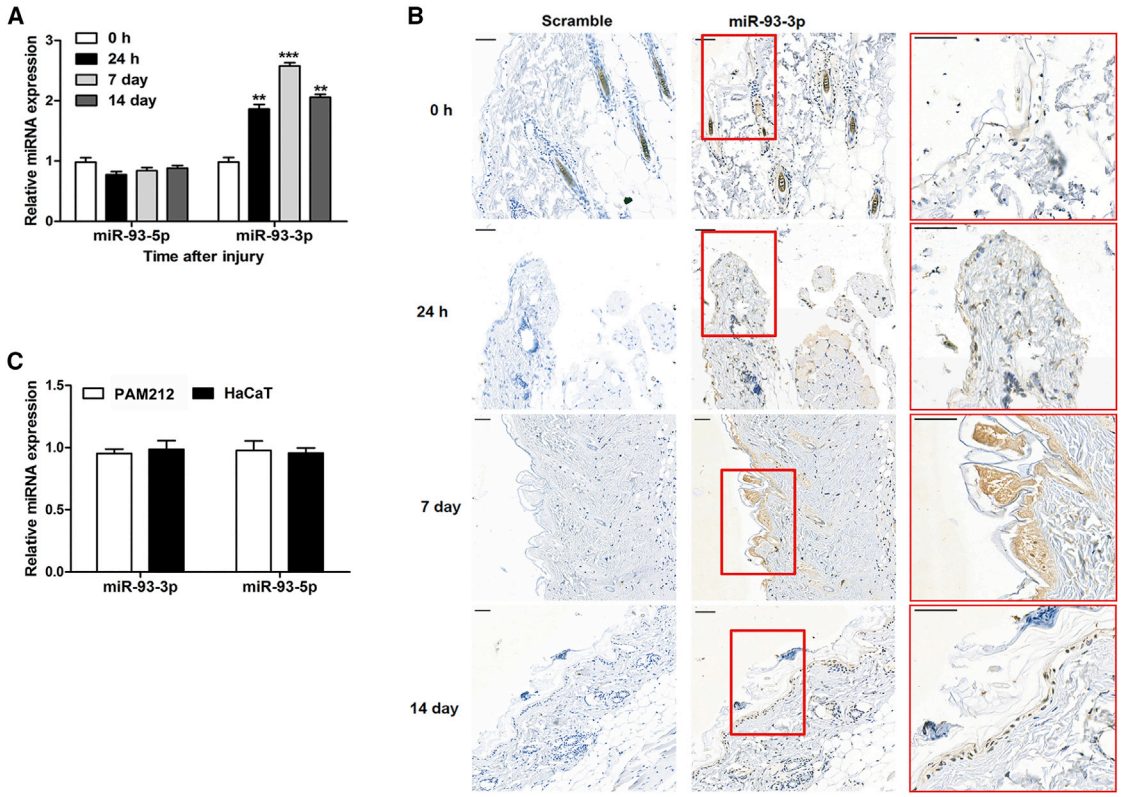

Figure 1. miR-93-3p upregulated during skin wound healing

(A) qRT-PCR for miR-93-3p and miR-93-5p in the wound edge tissue at indicated time points. (B) *In situ* hybridization was performed on wound biopsies using an miR-93-3p-specific probe or scrambled probe. Brown indicates miR-93-3p expression; black-purple indicates that it is expressed in the nucleus. Scale bars, 50 μm; n = 6. (C) qRT-PCR for miR-93-3p and miR-93-5p in the keratinocytes (PAM212 and HaCaT cell). Data are shown with mean ± SD. **p < 0.01, ***p < 0.001.

RESULTS

miR-93-3p is upregulated during wound healing of skin

We initially developed an *in vivo* surgical wound model in the mice skin and then isolated the surrounding tissue at varying time points postinjury. We further selected samples that represented the multiple sequential stages of wound healing, including hemostasis (0 h), inflammation (24 h), and proliferation (7th and 14th day). First, we measured the levels of miR-93-3p and miR-93-5p expression in mice wound edge tissue by quantitative reverse-transcriptase PCR (qRT-PCR) (Figure 1A). We found that miR-93-3p expression had increased significantly 24 h after the onset of wound healing, with an almost 2.5-fold greater increase in expression by 7 days. The relative expression levels decreased but remained significantly elevated at the 14th day, whereas there is no change in the expression of miR-93-5p during mice skin wound healing (Figure 1A). Therefore, we speculated that miR-93-3p plays an important role in the proliferation phase of skin wound healing. In order to reveal which cell type(s) are primarily responsible for the changes in miR-93-3p expression levels during wound healing, we performed *in situ* hybridization (ISH) with miR-93-3p (specific locked nucleic acid [LNA]-modified) probes on skin wound sections (Figure 1B). Epidermal keratinocytes were the primary location of the miR-93-3p signal. During the proliferative stage (7 days), miR-93-3p expression reached its peak at the 7th day; however, the expression levels significantly decreased at the 14th day after wound creation (Figure 1B). Further, we investigated the endogenous expression of miR-93-3p and miR-93-5p in keratinocytes (PAM212 and HaCaT cell). As shown in Figure 1C, miR-93-3p and miR-93-5p were expressed in both skin cell lines. Subsequently, the above-mentioned results from our qRT-PCR and ISH experiments indicate that the levels of miR-93-3p expression are highly regulated in wound edge epidermal keratinocytes, with an increase in expression in the inflammatory phase that peaked during the proliferative phase.

miR-93-3p promotes HaCaT cell proliferation and migration

Since miR-93-3p is positively upregulated in the keratinocytes, which are in a proliferative phase, we either overexpressed or inhibited miR-93-3p in HaCaT cells to explore the effects on proliferation. Initially, we confirmed the efficiency of miR-93-3p overexpression or inhibition through qRT-PCR (Figure 2A).

It was evident that the proliferation marker Ki-67 was upregulated when miR-93-3p was overexpressed, but its expression decreased when miR-93-3p was inhibited (Figure 2B). Further, we confirmed

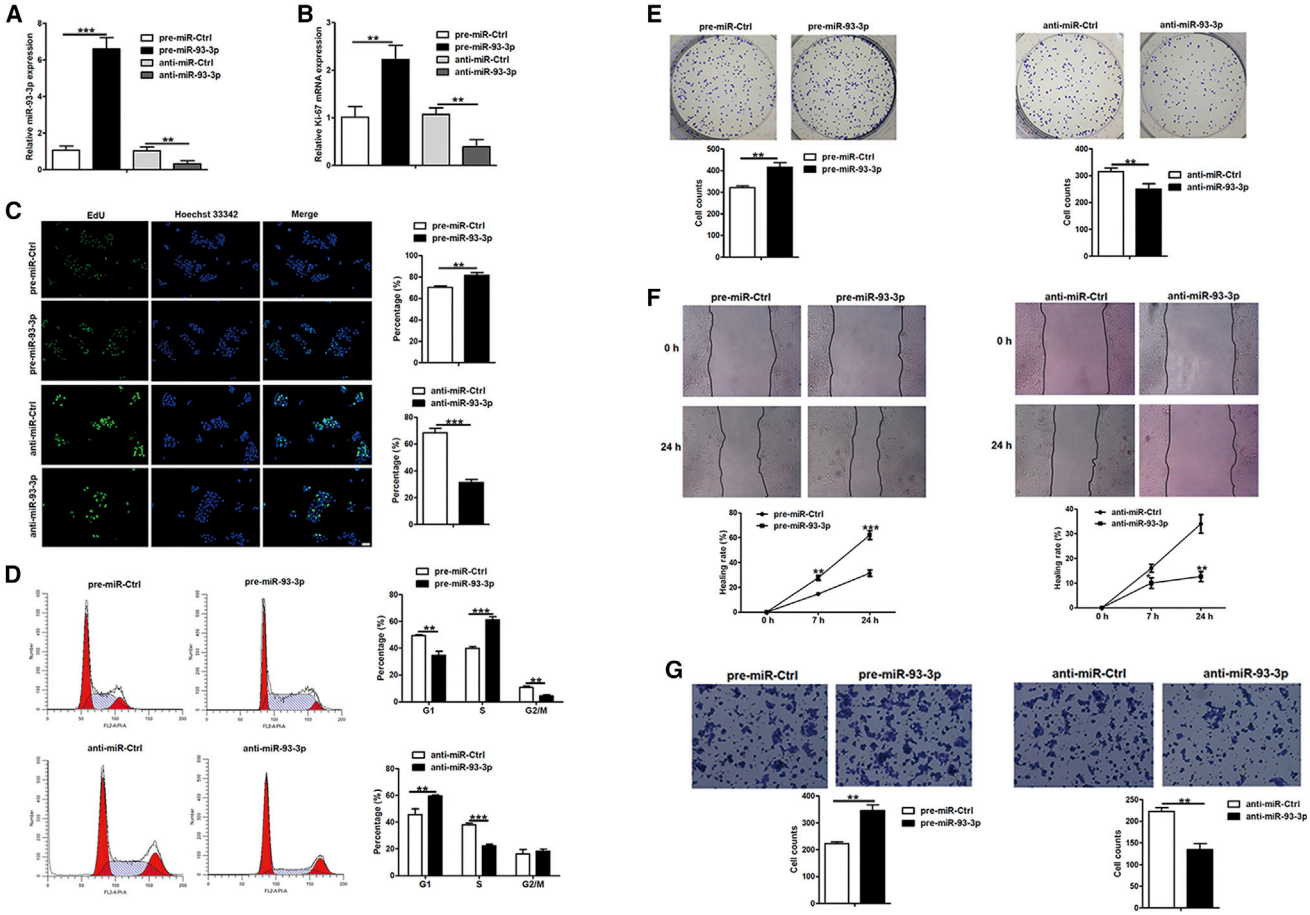

Figure 2. miR-93-3p promotes HaCaT cell proliferation and migration

HaCaT cells were transfected with 20 nM pre-miR-control (Ctrl), pre-miR-93-3p, anti-miR-Ctrl, or anti-miR-93-3p for 48 h. (A) qRT-PCR for miR-93-3p to test the transfection efficiency for miR-93-3p overexpression or inhibition. (B) The expression of proliferation marker Ki-67 was analyzed in the transfected HaCaT cells using qRT-PCR. (C) Cell proliferation measured by the EdU assay. Scale bar, 50 μm. Percentage of EdU+ cells is shown. (D) Cell-cycle analysis by flow cytometry. Percentage of cells in the G1, S, and G2/M phases of the cell cycle is shown. (E) Colony formation of the transfected HaCaT cells. (F) Scratch assays were performed to assess the migration of HaCaT cells. Photographs were taken at indicated time points after scratch injury. (G) Representative photographs of the Transwell migration assay for HaCaT cells. The number of cells passing through the membrane was counted. Data of one representative experiment out of four independent experiments are shown with mean ± SD. $^{**}p < 0.01$, $^{***}p < 0.001$.

our results using the 5-ethynyl-2′-deoxyuridine (EdU) assay. EdU-positive cells decreased with miR-93-3p inhibition, indicating a reduced cell proliferation (Figure 2C). In addition, flow cytometric cell-cycle analysis and colony-formation assays suggested that miR-93-3p stimulated keratinocytes growth over the long term (Figures 2D and 2E). Thus, it is evident that miR-93-3p positively regulates keratinocytes growth, as indicated by both the subsequent increase in progression of the cell cycle and promotion of long-term self-renewal.

Further, as keratinocytes migration is crucial to epidermal regeneration, we wanted to understand the role of miR-93-3p in keratinocytes migration. With the use of the scratch assay, we could observe that miR-93-3p overexpression increased healing of the wound significantly, 24 h postscratching. However, inhibition of the endogenous miR-93-3p significantly decreased the healing of the scratch (Figure 2F). Parallelly, we used the Transwell migration assay and observed that miR-93-3p overexpression increased the migration of HaCaT cells. Alternatively, miR-93-3p inhibition led to a decrease in the migration of HaCaT cells (Figure 2G). Our data collectively established miR-93-3p as a positive regulator of motility for HaCaT cells.

ZFP36L1 is targeted by miR-93-3p in HaCaT cells

Because miRNA affects the regulation of its target genes, we aimed to establish precisely the target gene that mediates the biological effects of miR-93-3p in keratinocytes. Through the TargetScan website (http://www.targetscan.org/vert_72/), we identified that ZFP36L1 was a possible target of miR-93-3p, and several previous studies had reported that ZFP36L1 inhibited cell proliferation and

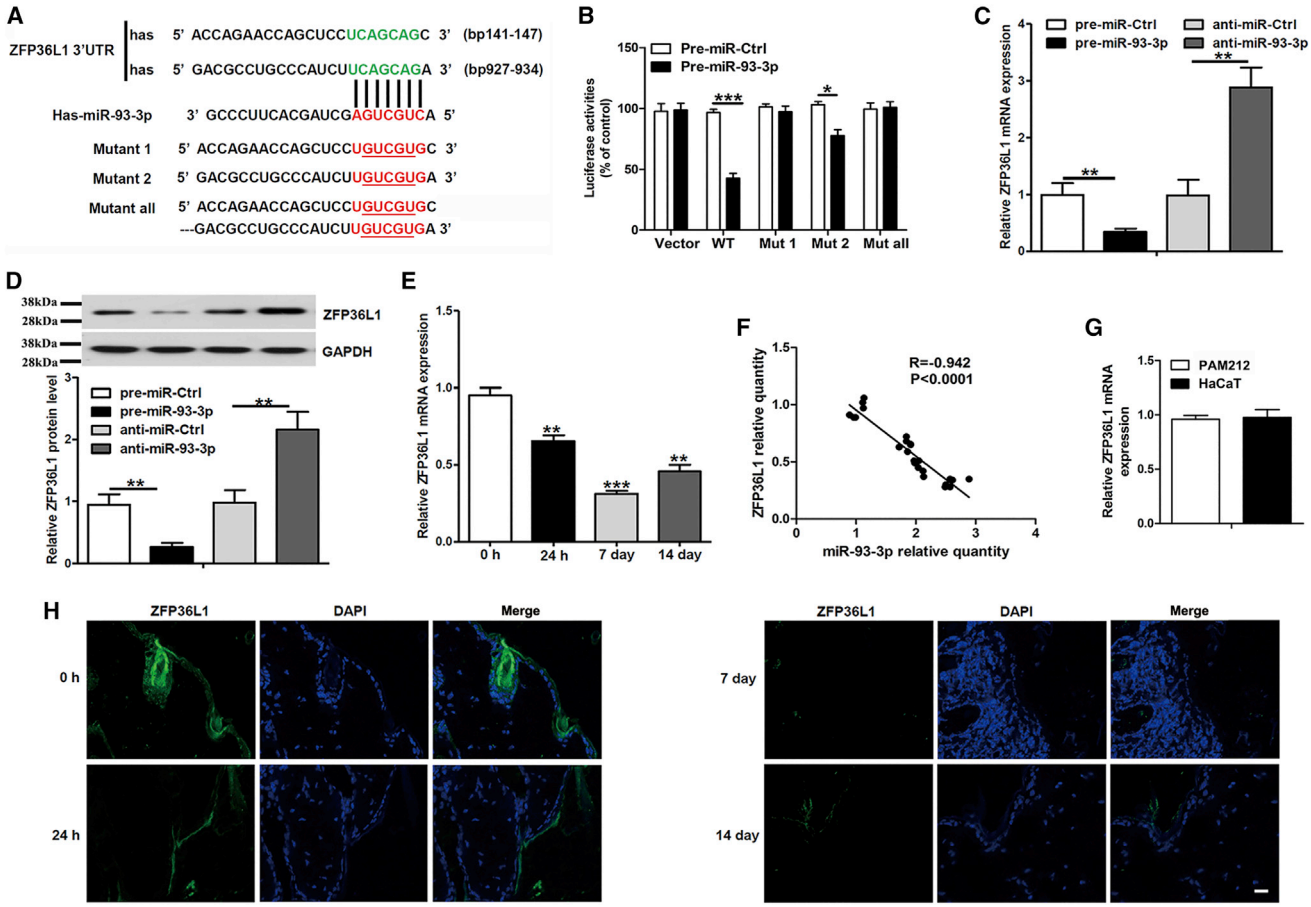

Figure 3. ZFP36L1 is targeted by miR-93-3p in HaCaT cells

(A) Alignment of miR-93-3p and its corresponding complementary binding sequence in the ZFP36L1 3′ UTR, as determined by the TargetScan bioinformatics algorithm. (B) HaCaT cells were transfected with 200 ng mL^{-1} luciferase reporter plasmid containing wild-type (WT) or mutant (Mut 1, Mut 2, and Mut all) ZFP36L1 3′ UTR or empty vector (Vector) together with 20 nM pre-miR-93-3p or pre-miR-Ctrl, and luciferase activity was measured 48 h later. (C and D) HaCaT cells were transfected with 20 nM pre-miR-93-3p/anti-miR-93-3p for 48 h, and ZFP36L1 expression was analyzed by qRT-PCR and western blot. (E) ZFP36L1 expression was analyzed by qRT-PCR in wound biopsies at the indicated time points. (F) Correlation analysis of ZFP36L1 and miR-93-3p in mouse wound biopsies by Pearson's correlation coefficient (n = 6). (G) qRT-PCR for ZFP36L1 in the keratinocytes (PAM212 and HaCaT cell). (H) Immunofluorescence staining of ZFP36L1 (green) in wound sections, which were counterstained using 4′,6-diamidino-2-phenylindole (DAPI; blue, nucleus). Scale bar, 50 μm. Data of one representative experiment out of four independent experiments are shown with mean ± SD. **p < 0.01, ***p < 0.001.

migration.[15–17] Hence, in the current study, we focused on ZFP36L1 as one of the target genes of miR-93-3p.

Initially, to understand if ZFP36L1 was a direct target of miR-93-3p, we used 3′ UTR luciferase reporter assays in HaCaT cells. Reporter gene constructs with the full-length 3′ UTR of ZFP36L1 mRNA were employed in HaCaT cells (Figures 3A and 3B). In cells with the wild-type ZFP36L1, miR-93-3p overexpression significantly downregulated the 3′ UTR luciferase activity. Additionally, a clear, significant decrease in luciferase activity could be observed in the presence of pre-miR-93-3p with the aid of the reporter construct containing the mutant (Mut) 2 clone. Further, this decrease in luciferase activity could be inversed in the presence of ZFP36L1 3′ UTR that affected either Mut 1 or both Mut 1 and Mut 2 (Mut all). Hence, we could clearly estimate that the region between 141 to 147 bp is the important region that is essential for miR-93-3p binding in the 3′ UTR of ZFP36L1. Above-mentioned data indicate that ZFP36L1 expression is regulated by the direct binding of miR-93-3p to the predicted target site in the 3′ UTR of ZFP36L1. Parallelly, we also observed that in HaCaT cells, overexpression of miR-93-3p decreased ZFP36L1 expression significantly. However, inhibition of miR-93-3p caused an upregulation of ZFP36L1 at both the mRNA (Figure 3C) and protein level (Figure 3D). Further, with the *in vivo* wounds, which were collected from our animal models, we checked the expression levels of ZFP36L1 at different stages of the healing process. After injury, the expression of ZFP36L1 began to decline, with the most severe decrease on the 7th day postinjury, but its expression gradually increased by day 14; however, the level was still lower than the control, unwounded sample, as detected by qRT-PCR (Figure 3E).

Clearly, we observed a negative correlation ($R = -0.89$, $p < 0.0001$) between the ZFP36L1 expression and miR-93-3p levels in wound samples postinjury (Figure 3F). Additionally, we investigated the endogenous expression of ZFP36L1 in keratinocytes (PAM212 and HaCaT cell). As shown in Figure 3G, ZFP36L1 was expressed in both skin cell lines. Next, with the aid of immunofluorescence staining, it was evident that ZFP36LI protein was present in all of the multiple layers of epidermal keratinocytes in the unwounded mouse skin. Additionally, ZFP36L1 expression decreased significantly in the wounded skin on the 7th day, similar to the qRT-PCR data (Figure 3H). These alternating expression patterns between the miR-93-3p and ZFP36L1, as observed in both our *in vitro* and *in vivo* experiments, confirm that miR-93-3p targets ZFP36L1 in keratinocytes. Additionally, it could be inferred that the upregulated miR-93-3p expression may be the key factor in the reduction of ZFP36L1 levels during the wound healing of skin.

Silencing of ZFP36L1 promotes HaCaT cell proliferation and migration

The role of ZFP36L1 in wound healing is largely unclear, and to understand whether the proproliferative and promigratory effects of miR-93-3p are through ZFP36L1, we performed silencing experiments by transfecting control short hairpin (sh)RNA or ZFP36L1 shRNA on HaCaT cells. We measured the silencing efficiency using qRT-PCR (Figure 4A) and western blot (Figure 4B). Reduced expression of ZFP36L1 by shRNA resulted in a significant upregulation in the proliferation marker Ki-67 levels (Figure 4C). We also observed an increased percentage of EdU-positive cells with inhibition of ZFP36L1 expression (Figure 4D). Through cell-cycle progression analysis by flow cytometry and colony-formation assays (Figures 4E and 4F), our results confirmed that ZFP36L1 inhibits keratinocyte proliferation. Based on the results from both the scratch assay and Transwell migration assay, it was clear that silencing of ZFP36L1 increased the HaCaT cell's migratory capacity (Figures 4G and 4H). Therefore, the above data indicate that the silencing of ZFP36L1 promotes proliferation and migration of HaCaT cells.

ZFP36L1 affects ZFX expression in HaCaT cells

ZFP36L1, a widely studied RBP, encompasses two tandem repeats of zinc finger motifs with a gene expression regulatory function at the post-transcriptional level. This is achieved by the unique binding of ZFP36L1, specifically to the adenine uridine (AU)-rich elements (AREs) in the 3′ UTR of the mRNAs, thereby causing ARE-dependent mRNA decay.[18] ZFP36L1 has been shown to function in multiple biological processes by targeting a wide overlapping range of mRNAs. Moreover, ZFX has been shown to promote the proliferation and migration of liver cancer cells.[19] Therefore, we focused on ZFX in this study. Further, we could identify six AUUUA sequence motifs with the aid of the ARE database (https://brp.kfshrc.edu.sa/ARED/) in the 3′ UTR region of ZFX mRNA (Figure 5A). Consecutively, to understand further the physical associations between ZFP36L1 with ZFX 3′ UTR, we performed RNA immunoprecipitation assays using anti-ZFP36L1 antibody. The products were amplified with qRT-PCR employing the primers that flank the UTR1−5 regions of the ZFX 3′ UTR. The primers flanking the ZFX 3′ UTR6 failed to amplify the immunoprecipitated product. This suggested that the AREs that are present in UTR2, and not in the UTR6, are vital to allow ZFP36L1 and ZFX 3′ UTR binding (Figures 5B and 5C). To confirm this, we performed pull down of ZFP36L1 after exogenous expression of either ZFX 3′ UTR wild-type or with mutation at the UTR2 site (Figure S1).

Further, we were interested to understand the effect of ZFP36L1 overexpression on ZFX expression. To achieve this, we performed immunoblotting analysis with the lysate obtained from HaCaT cells that were transfected with increasing concentrations of ZFP36L1, and it was evident that as ZFP36L1 levels increased, a decrease in ZFX protein level could be observed (Figure 5D). Additionally, with the ZFP36L1 transfected (increasing concentrations at 0.5, 1.0, and 1.5 μg) HaCaT cell lysates, we performed an RNA immunoprecipitation assay, and it was evident that there was a dose-dependent decrease in binding of ZFP36L1 to 3′ UTR of ZFX (Figure 5E). Loss-of-function assays were also performed to further elucidate the role of ZFP36L1. First, ZFP36L1 silencing was accomplished using target-specific shRNA transfection in HaCaT cells, and the silencing efficacy was validated with the use of an antigen-specific antibody. Evidentially, silencing of ZFP36L1 significantly increased the ZFX expression (Figure 5F), which was similar to the results obtained from the RNA immunoprecipitation assay (Figure 5G). Hence, the evidence indicates the vital role of ZFP36L1 in maintaining the mRNA stability of ZFX and thus, regulating its expression in the HaCaT cells.

ZFX promotes HaCaT cell proliferation and migration

Previous literature indicates that ZFX promotes cell proliferation and migration,[19] but whether it promotes keratinocyte proliferation and migration remains unclear. In order to identify whether ZFX has a function in keratinocytes, we first investigated the endogenous expression of ZFX in keratinocytes (PAM212 and HaCaT cell). As shown in Figure 6A, ZFX was expressed in both skin cell lines, and then, we overexpressed or inhibited ZFX in the HaCaT cells with transfection empty vector, ZFX overexpression, shRNA control, or shRNA ZFX plasmids. qRT-PCR (Figure 6B) and western blot analysis (Figure 6C) were used to confirm the efficacy of overexpression or silencing of ZFX. Interestingly, it was evident that ZFX overexpression increased Ki-67 expression in HaCaT cells, and inhibition of ZFX led to a reduction in Ki-67 levels (Figure 6D). EdU staining also showed similar results, indicating that ZFX has a positive effect on proliferation (Figure 6E). Further confirmation of our results was obtained by checking the cell-cycle progression using flow cytometry, along with colony-formation assays (Figures 6F and 6G). Thus, these results confirm that ZFX is a proproliferative factor of keratinocytes.

To subsequently confirm its migration and healing capacity, cells overexpressing ZFX were used to perform the scratch assay. Evidentially, 24 h after scratching, HaCaT cells overexpressing ZFX showed increased healing. However, cells with inhibition of ZFX showed opposite results 24 h postscratching (Figure 6H). Subsequently, we also performed Transwell assays to assess the migratory capacity of these cells. Similar to the scratch assay results, cells overexpressing ZFX showed significantly increased migration, whereas cells with

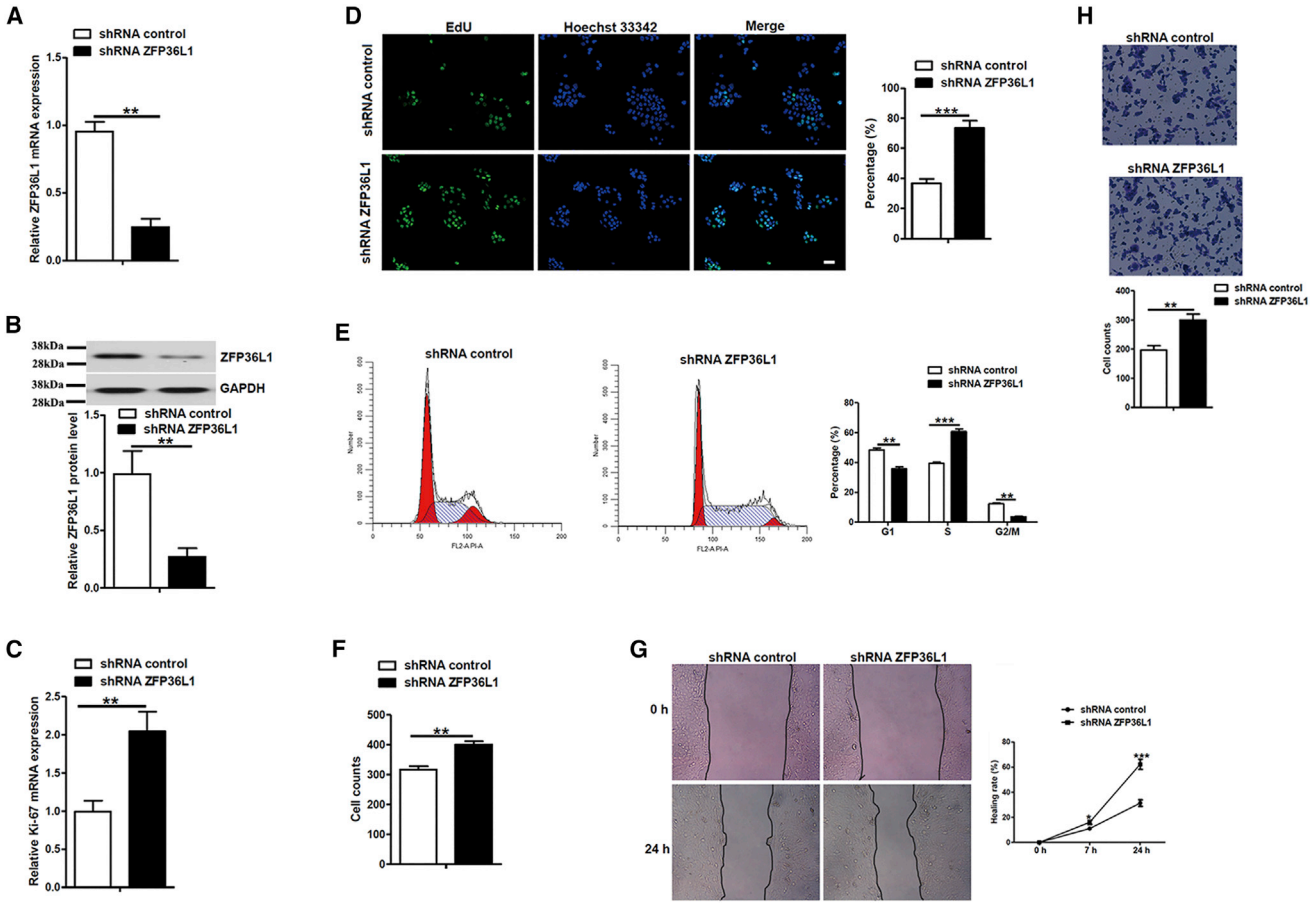

Figure 4. Silencing of ZFP36L1 promotes HaCaT cell proliferation and migration

HaCaT cells were transfected with 20 nM shRNA control or shRNA ZFP36L1 for 48 h. (A and B) The silencing efficiency was analyzed by measuring ZFP36L1 levels with qRT-PCR and western blot. (C) The expression of proliferation marker Ki-67 was analyzed in the transfected HaCaT cells using qRT-PCR. (D) Cell proliferation was measured by the EdU assay. Scale bar, 50 μm. The percentages of EdU+ cells are shown. (E) Cell-cycle analysis by flow cytometry. The percentages of cells in the G1, S, and G2/M phases of the cell cycle are shown. (F) Colony formation of the transfected HaCaT cells. (G) Scratch assays were performed to assess the migration of the transfected HaCaT cells. Photographs were taken at the indicated time points after scratch injury. (H) Representative photographs of the Transwell migration assay for the transfected HaCaT cells. The number of cells passing through the membrane was counted. Data of one representative experiment out of four independent experiments are shown with mean ± SD. $^{**}p < 0.01$, $^{***}p < 0.001$.

inhibition of ZFX showed significantly decreased HaCaT cell migration (Figure 6I). These results confirmed our hypothesis that ZFX positively regulated the migration of HaCaT cells.

miR-93-3p promotes keratinocyte proliferation and migration by upregulating ZFX expression

Whether ZFX was involved in the promotion of the miR-93-3p/ZFP36L1 axis in keratinocyte proliferation and migration was further investigated. We transfected these cells with pre-miR-93-3p, ZFP36L1, or pre-miR-93-3p + ZFP36L1 for 48 h and measured ZFX expression levels using qRT-PCR (Figure 7A) and western blotting (Figure 7B). Cells transfected with only pre-miR-93-3p had 4-fold upregulated ZFX mRNA expression than in control cells, and when cotransfected with ZFP36L1, ZFX levels were still high but lower than in cells with pre-miR-93-3p only. Additionally, transfection with just ZFP36L1 slightly decreased ZFX expression with respect to the control (Figure 7A). Western blot experiments showed that the same phenomena occurred at the protein level (Figure 7B).

Additionally, we measured the expression levels of Ki-67 by qRT-PCR and found that proliferation was significantly decreased in ZFP36L1 + pre-miR-93-3p-transfected cells and then in cells transfected with pre-miR-93-3p alone, which was nevertheless greater than control levels (Figure 7C). We also observed that ZFP36L1 + pre-miR-93-3p-transfected cells had the weakest proliferation ability, as observed by the decreased percentage of cells positive for EdU (Figure 7D). Similar results were found for cell-cycle analysis by flow cytometry and colony-formation assays (Figures 7E and 7F). Additionally, the observations from the scratch assay and Transwell migration assay showed that ZFP36L1 + pre-miR-93-30-transfected cells strikingly

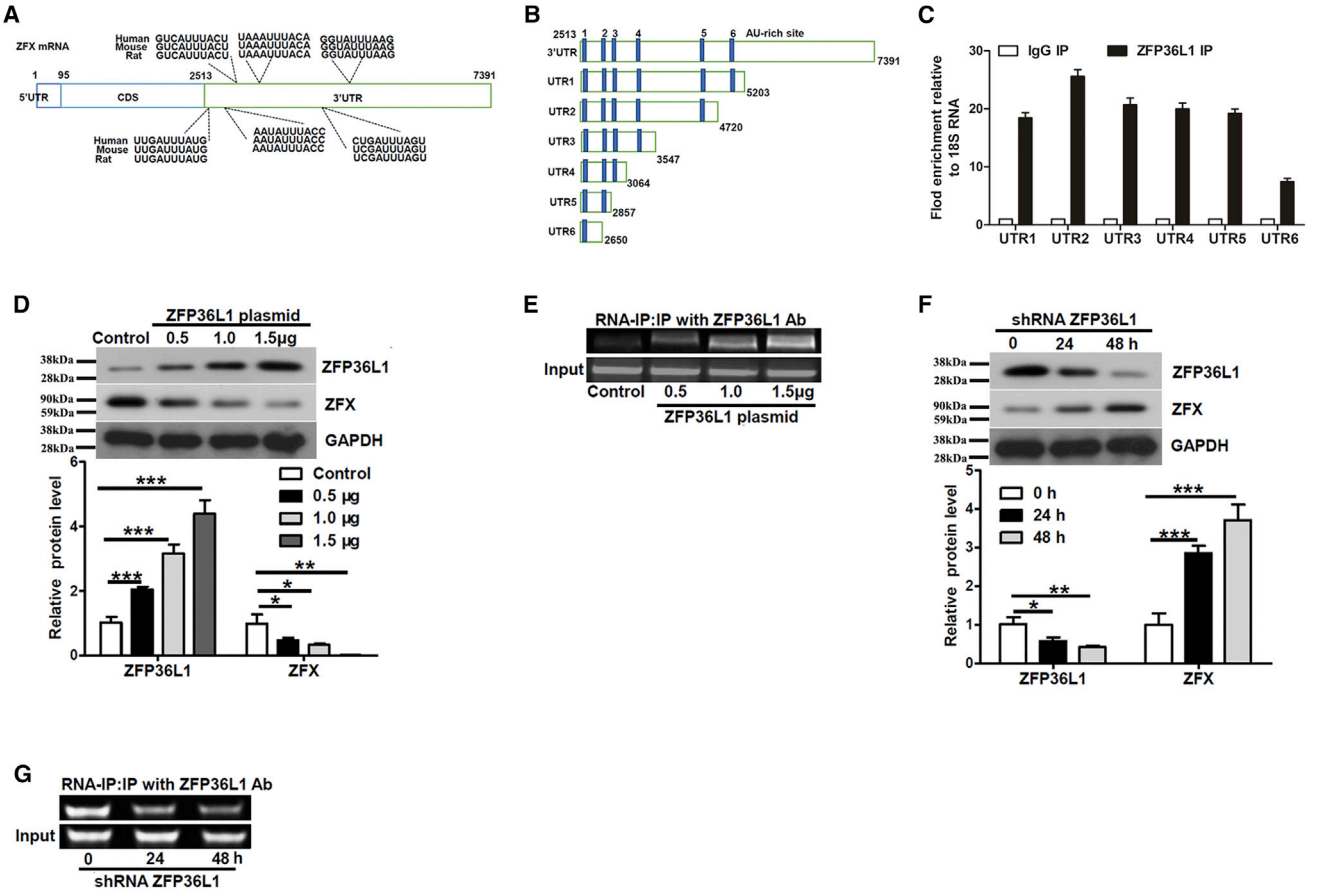

Figure 5. ZFP36L1 affects ZFX expression in HaCaT cells

(A) Six conserved AU-rich elements located in the 3′ UTR of ZFX transcripts of humans and mice. The sequence and location of the AU-rich elements are presented as a graphic. (B) Schematic representation of the UTR1–UTR6 regions. (C) RT-PCR quantification of RNA immunoprecipitations (IPs). Association of ZFP36L1 with ZFX 3′ UTR regions (UTR1, UTR2, UTR3, UTR4, UTR5, and UTR6). Whole-cell lysates from HaCaT cells were used for immunoprecipitation using anti-ZFP36L1 antibody or nonspecific IgG. Total RNA was extracted from immunoprecipitated complexes, reverse transcribed, and subjected to PCR analysis using primers to amplify the UTR1–UTR6 regions of ZFX 3′ UTR. The negative control was IgG (mouse). Glyceraldehyde 3-phosphate dehydrogenase expression was determined (input) to ensure that equal amounts of samples were taken during the RNA immunoprecipitation experiment. (D) HaCaT cells were transiently transfected for 48 h with ZFP36L1 plasmid (control, 0.5, 1.0, or 1.5 μg) and were then immunoblotted for ZFP36L1 and ZFX protein expression. (E) HaCaT cells were transiently transfected for 48 h with ZFP36L1 plasmid (control, 0.5, 1.0, or 1.5 μg), and RNA immunoprecipitation was performed using an anti-ZFP36L1 antibody. Total RNA was extracted from the immunoprecipitated complexes, reverse transcribed, and subjected to PCR analysis using ZFX 3′ UTR2 primers and densitometric analysis. (F) HaCaT cells were transiently transfected with shRNA ZFP36L1 (0, 24, and 48 h) and were then immunoblotted for ZFP36L1 and ZFX protein expression. (G) HaCaT cells were transiently transfected with shRNA ZFP36L1 (0, 24, and 48 h), and RNA immunoprecipitation was performed using anti-ZFP36L1 antibody. Total RNA was extracted from the immunoprecipitated complexes, reverse transcribed, and subjected to PCR analysis using ZFX 3′ UTR2 primers and densitometric analysis. Data of one representative experiment out of four independent experiments are shown with mean ± SD. *$p < 0.05$, **$p < 0.01$, ***$p < 0.001$.

decreased the migration capacity of HaCaT cells, whereas pre-miR-93-3p transfection led to a significant increase in migration of HaCaT cells (Figures 7G and 7H). Overall, observations from the current study indicate that miR-93-3p promotes keratinocyte proliferation and migration by upregulating ZFX expression.

Inhibition of miR-93-3p delays skin wound healing *in vivo*

Finally, with the use of the *in vivo* model, we studied the effects of miR-93-3p expression on wound healing. Mice were administered with a subcutaneous injection of miR-93-3p inhibitors or control oligos and treated with or without control shRNA (Ad-shC) or Ad-shZFP36L1. We found that wounds treated with anti-miR-93-3p showed significantly delayed wound closure compared with the rate of control-treated wounds, whereas wounds treated with Ad-shZFP36L1 showed significantly faster wound closure compared to the Ad-shC-treated wounds. Additionally, we found that the downregulation of ZFP36L1 expression reversed the delay in wound healing caused by anti-miR-93-3p (Figure 8A).

Further, when we analyzed the wound-edge skin after 7 days of injury, we observed that using anti-miR-93-3p did successfully decrease the

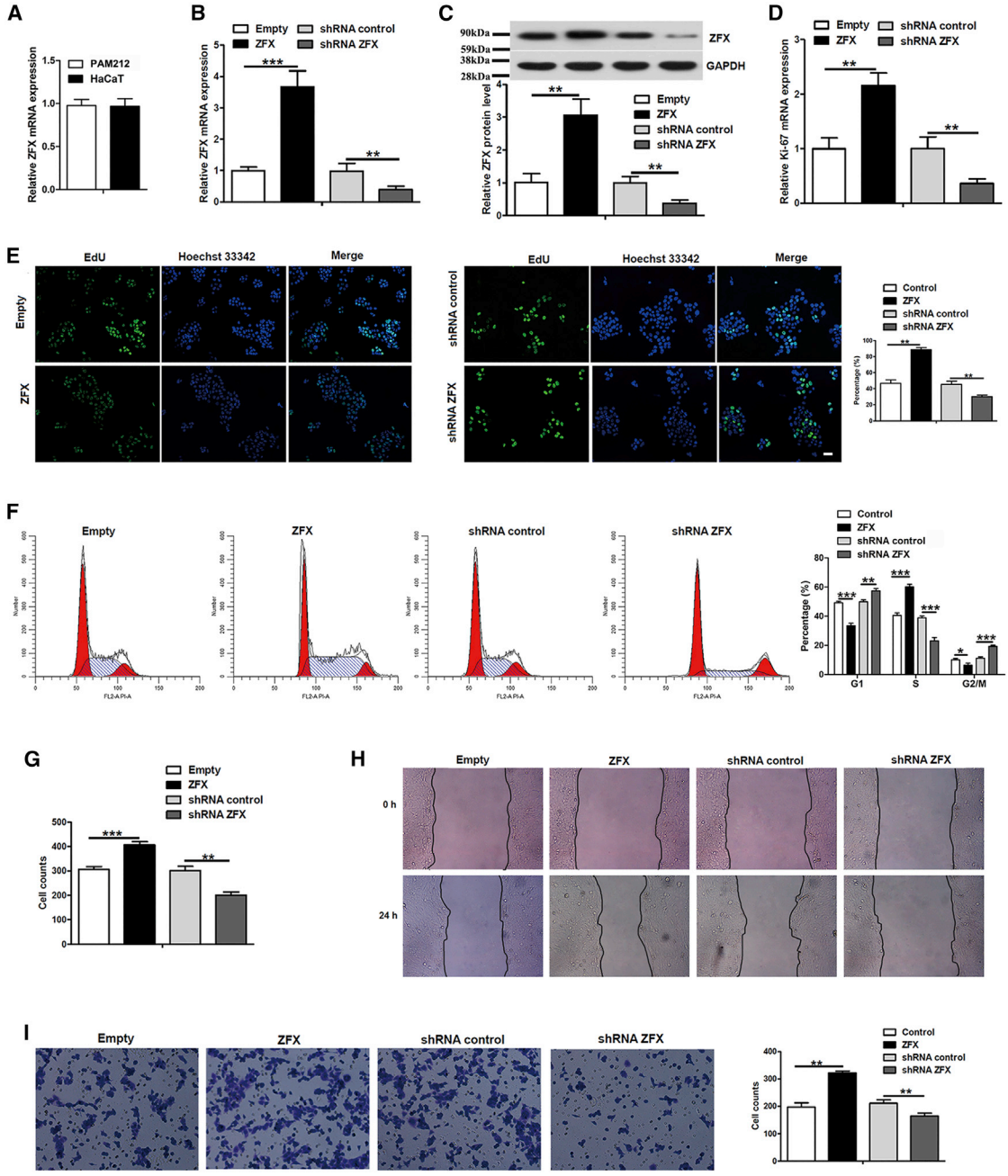

Figure 6. ZFX promotes HaCaT cell proliferation and migration

HaCaT cells were transfected with 20 nM empty vector, ZFX, shRNA control, or shRNA ZFX plasmid for 48 h. (A) qRT-PCR for ZFX in the keratinocytes (PAM212 and HaCaT cell). (B and C) qRT-PCR and western blot for ZFX to test the transfection efficiency for ZFX overexpression or inhibition. (D) The expression of proliferation marker Ki-67 was analyzed in the transfected HaCaT cells using qRT-PCR. (E) Cell proliferation was measured by the EdU assay. Scale bar, 50 μm. The percentages of EdU+ cells are shown. (F) Cell-cycle analysis by flow cytometry. The percentages of cells in the G1, S, and G2/M phases of the cell cycle are shown. (G) Colony formation of the transfected HaCaT cells. (H) Scratch assays were performed to assess the migration of HaCaT cells. Photographs were taken at the indicated time points after scratch injury. (I) Representative photographs of the Transwell migration assay for HaCaT cells. The number of cells passing through the membrane was counted. Data of one representative experiment out of four independent experiments are shown with mean ± SD. *$p < 0.05$, **$p < 0.01$, ***$p < 0.001$.

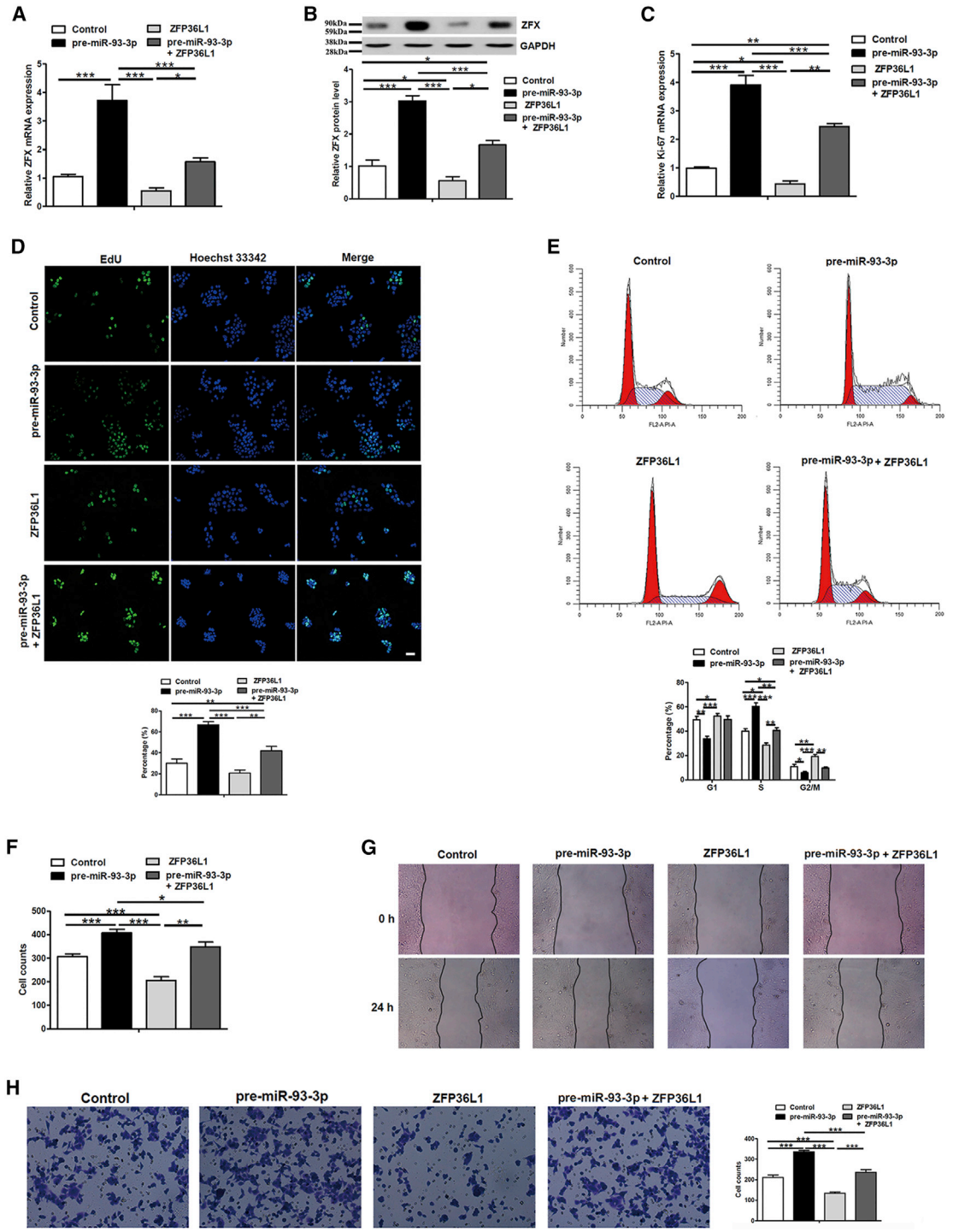

Figure 7. miR-93-3p promotes HaCaT cell proliferation and migration by upregulating ZFX expression

HaCaT cells were transfected with 20 nM pre-miR-93-3p, ZFP36L1, or pre-miR-93-3p + ZFP36L1 for 48 h. (A and B) The expression of ZFX was determined by qRT-PCR and western blot. (C) The expression of proliferation marker Ki-67 was analyzed in the transfected HaCaT cells using qRT-PCR. (D) Cell proliferation was measured by the EdU assay. Scale bar, 50 μm. The percentages of EdU+ cells are shown. (E) Cell-cycle analysis was performed by flow cytometry. The percentages of cells in the G1, S, and G2/M phases of the cell cycle are shown. (F) Colony formation of the transfected HaCaT cells. (G) Scratch assays were performed to assess the migration of HaCaT cells. Photographs

(legend continued on next page)

expression levels of miR-93-3p (Figure 8B) when compared to control. However, anti-miR-93-3p significantly increased ZFP36L1 protein levels (Figure 8C) and decreased ZFX protein levels (Figure 8D) when compared to those in the control wounds. Alternatively, the silencing of ZFP36L1 did not cause any change in miR-93-3p levels (Figure 8B). We further confirmed that the use of Ad-shZFP36L1 did significantly decrease ZFP36L1 levels and increase ZFX protein levels (Figures 8C and 8D). Finally, we found that use of anti-miR-93-3p significantly decreased the Ki-67 levels, whereas silencing of ZFP36L1 significantly increased the Ki-67 levels (Figure 8E). Hence, from the above-mentioned results, it is evident that ZFP36L1 is a direct target of miR-93-3p, and ZFX is, in turn, regulated by ZFP36L1. Additionally, we can infer that the loss of miR-93-3p expression causes a delay in skin wound healing, whereas downregulation of ZFP36L1 expression reversed the delay in wound healing caused by anti-miR-93-3p. This study demonstrates that miR-93-3p regulates wound healing through the regulation of ZFP36L1 and ZFX.

DISCUSSION

With the use of an *in vivo* mouse skin wound-healing model, we demonstrated that the expression of miR-93-3p is upregulated in epidermal wound keratinocytes through the inflammatory phase (1-day postinjury) to the proliferative phase (7 days postinjury). However, we observed no change in the expression of miR-93-5p during mice skin wound healing. *In vitro* studies using cultured HaCaT cells indicated that miR-93-3p overexpression enhances cell proliferation and migration; however, miR-93-3p inhibition has opposing effects. miR-93-3p binds and inactivates ZFP36L1, causing upregulation of ZFX and subsequent stimulation of keratinocyte proliferation and migration. To the best of our knowledge, this is the first study to mechanistically elucidate the role of miR-93-3p in the regulation of wound healing.

Many previous studies have indicated that miRNAs play a crucial role in the proliferation and migration of keratinocytes. A study showed that miR-330-5p could regulate proliferation and migration of keratinocytes by targeting Pdia3.[20] Yu et al.[21] showed that miR-26a regulates proliferation and migration of keratinocytes by modulating the PTEN/AKT signaling pathway. Similarly, miRNA-126 was observed to regulate proliferation and migration of keratinocytes by regulating the phosphatidylinositol 3-kinase (PI3K)/AKT signaling pathway.[22] In the current study, we identified that miR-93-3p plays an important role in wound healing by enhancing proliferation and migration of keratinocytes by using multiple functional assays. However, the ability of miR-93-3p to promote cell proliferation and migration has been previously reported by Wang et al.[23], where they showed that miR-93-3p was substantially upregulated in clear cell renal cell carcinoma and that this upregulation stimulated proliferation, metastasis, and invasion. Similarly, another study by Li et al.[24] also showed that the miR-93-3p expression was upregulated in cervical cancer cells, which promoted the invasion and cell-cycle entry of the cancer cells. Taken together, our findings have, for the first time, shown that miR-93-3p facilitates the proliferation and migration of keratinocytes and may be beneficial to the healing of skin wounds.

Since it is well known that miRNAs exert their biological functions primarily by inhibiting the expression of target genes,[25] in this study, we aimed to prove that ZFP36L1 was the target gene of miR-93-3p. Christine Hacker et al.[26] showed that ZFP36L1 plays an important role in wound healing by regulating vascular endothelial growth factor (VEGF) mRNA stability. However, whether ZFP36L1 is involved in keratinocytes proliferation and migration during wound healing has not been investigated. Some studies show that ZFP36L1 promotes tumor development by promoting cell proliferation and migration, for example, hepatocellular carcinoma[27] and glioblastoma.[17] However, other studies suggested that ZFP36L1 may function as a tumor suppressor through the inhibition of cell proliferation and migration in many cancers such as, lung carcinoma[28] and colorectal cancer.[16] This suggests that ZFP36L1 may have different biological functions in different diseases. In our study, we proved that ZFP36L1 was the target gene of miR-93-3p. Furthermore, our study showed that the silencing of ZFP36L1 promotes proliferation and migration of keratinocytes. Taken together, our data strongly suggest that ZFP36L1 is a key target facilitating the biological functions of miR-93-3p in keratinocytes during skin wound healing.

ZFP36L1 is an RBP that is also involved in intracellular regulatory processes by binding to the AREs found in the 3′ UTRs of mRNA, triggering decay of the mRNA.[29] Son et al.[30] showed that the knockdown of ZFP36L1 upregulated the mRNA expression of two heat shock protein 70 family members, which in turn, inhibited chondrocyte apoptosis in osteoarthritis. Similarly, we performed RNA immunoprecipitation and western blot to verify that ZFP36L1 affects the stability of ZFX's mRNA and inhibits its expression. In addition, with the use of several functional assays in HaCaT cells with modified ZFX expression, we demonstrate that ZFX promotes proliferation and migration, which is similar to the results from the Li et al.[31] study and Bao et al.[32] study. By modifying the expressions of miR-93-3p and ZFP36L1 in HaCaT cells, we further confirmed that ZFX was involved in the promotion of the miR-93-3p/ZFP36L1 axis, which in turn, regulated the proliferation and migration of keratinocytes. Therapeutic miRNAs have been identified, and their effectiveness has been validated *in vivo*, predominantly in cancer research.[33–35] In this study, we intradermally injected miR-93-3p inhibitors or control oligos into the wound edges of an *in vivo* model and demonstrated the therapeutic effect of miR-93-3p in skin wound healing.

We have shown that the miR-93-3p/ZFP36L1/ZFX axis plays an important role in skin wound healing by regulating the proliferation and migration of keratinocytes through a series of *in vivo* and *in vitro* experiments.

were taken at the indicated time points after scratch injury. (H) Representative photographs of the Transwell migration assay for HaCaT cells. The number of HaCaT cells passing through the membrane was counted. Data of one representative experiment out of four independent experiments are shown with mean ± SD. *$p < 0.05$, **$p < 0.01$, ***$p < 0.001$.

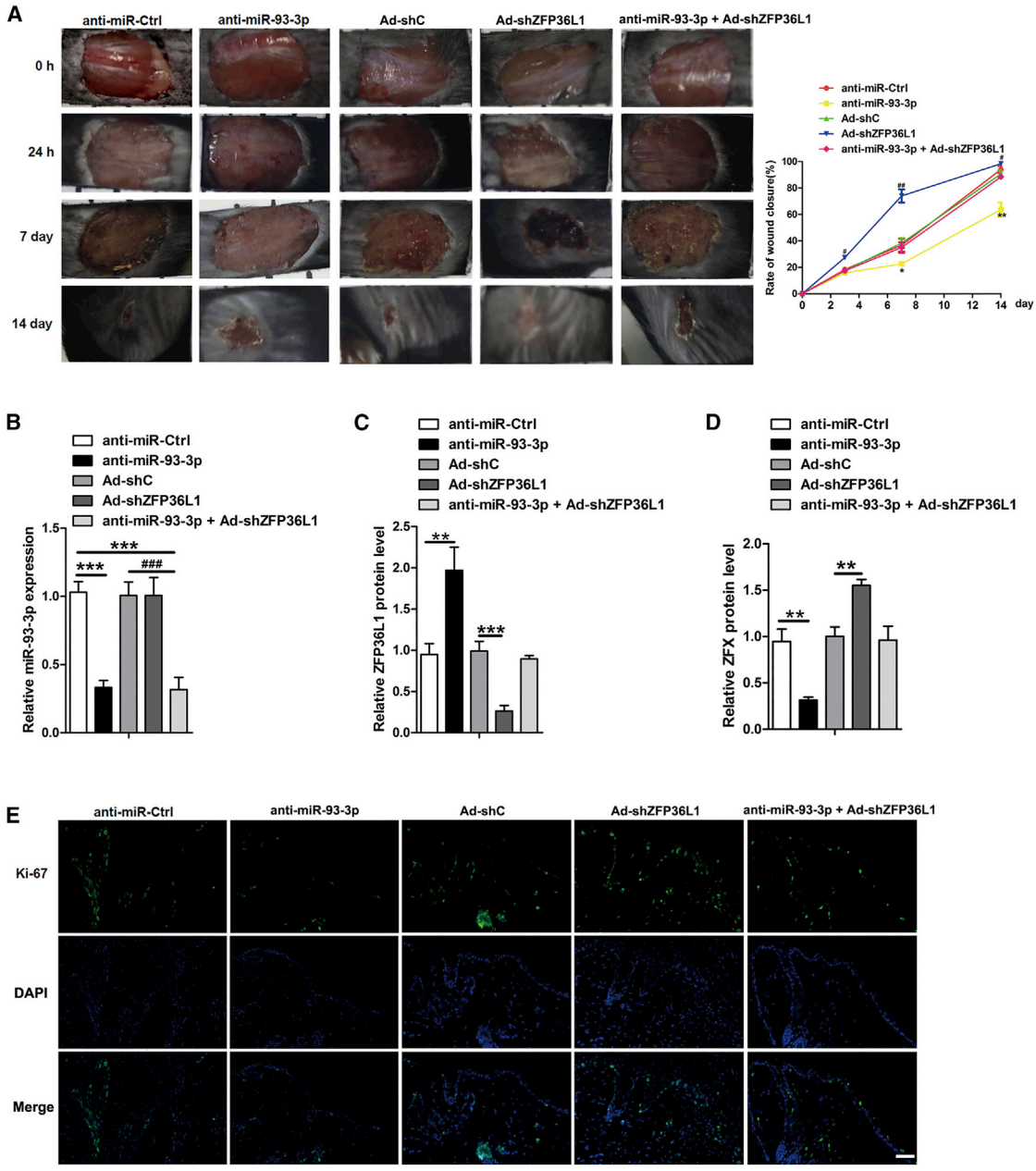

Figure 8. Inhibition of miR-93-3p delays skin wound healing *in vivo*

Skin wounds were treated with anti-miR-Ctrl or anti-miR-93-3p and treated with or without control shRNA (Ad-shC) or Ad-shZFP36L1 for 14 days. (A) Left: representative images of treated wounds at 0 h, 24 h, 7 days, and 14 days postwound-injury. Right: level of wound closure is expressed as a percentage of the wound area from the initial wound area. (B–D) The expression of miR-93-3p, ZFP36L1, and ZFX, respectively, was analyzed by qRT-PCR in the wound-edge skin 7 days after injury. (E) Immunofluorescence staining for Ki-67 (green) in the wound-edge skin 7 days after injury, which was counterstained using DAPI (blue, nucleus). Scale bar, 50 μm; n = 6. Data are shown with mean ± SD. *p < 0.05, **p < 0.01, ***p < 0.001 versus anti-miR-Ctrl #p < 0.05, ##p < 0.01, ###p < 0.001 versus Ad-shC.

MATERIALS AND METHODS

Cell culture and treatment

HaCaT cells were obtained from the American Type Culture Collection (ATCC), whereas Dulbecco's modified Eagle's medium (DMEM) and fetal bovine serum (FBS) were purchased from HyClone (Logan, UT, USA), and penicillin/streptomycin (P/S) was from Gibco (Carlsbad, CA, USA). HaCaT cells were cultured in DMEM containing 10% FBS and 1% P/S at 37°C in a 5% CO_2 atmosphere.

In vivo wound experiments

We purchased 6-week-old C57BL/6 mice from Shanghai Laboratory Animal Center (SLAC). The mice were anesthetized using isoflurane prior to wound creation. We created full-thickness excision wounds (1×1.5 cm^2) by using forceps and surgical scissors. After wounding, mice were randomly divided into five groups: mice were administered with (1) a subcutaneous injection of 1 nmol negative control (NC; anti-miR-Ctrl) (Exiqon) from day 0 (immediately following the procedure) to day 14, with injections administered every second day; (2) 1 nmol LNA miR-93-3p inhibitor (anti-miR-93-3p) (Exiqon) from day 0 (immediately following the procedure) to day 14, with injections administered every second day; (3)Adenovirus injection the Ad-shC (10^{10} plaque-forming units [PFUs] in a total volume of 50 μL), purchased from Vector Labs, with injections administered only once, 2 days before modeling; (4) Ad-shZFP36L1 (10^{10} PFUs in a total volume of 50 μL), purchased from Vector Labs, with injections administered only once, 2 days before modeling; and (5) 1 nmol LNA miR-93-3p inhibitor (anti-miR-93-3p) (Exiqon) and Ad-shZFP36L1 (10^8 PFUs in a total volume of 50 μL).

An Olympus camera was used to photograph the wounds at 0 h, 24 h, 7^{th} day, and 14^{th} day after the creation of the wound. The wound-closure rate, i.e., percentage of wound reduction from the original wound, was deduced with the following formula: wound closure rate = wound area at day 0 − wound area at day "n" (n = 3, 7, 14) × 100% wound area at day 0. The mice were euthanized using CO_2 after sampling.

The Institutional Animal Care and Use Committee of Zhejiang Provincial People's Hospital reviewed and approved all of the procedures used in this study. All experiments were conducted according to guidelines approved by the Zhejiang Provincial People's Hospital.

Immunofluorescence staining

Each tissue section was sequentially deparaffinized, then rehydrated, and washed in phosphate-buffered saline (PBS). Subsequently, to unmask the antigen, tissue sections were microwaved in 10 mM sodium citrate buffer and washed with PBS. Sections were further incubated overnight with the primary antibodies toward ZFP36L1 (Proteintech; 12306-1-AP, 1:200) and Ki-67 (Servicebio; GB13030-2, 1:200) at 4°C, followed by goat anti-rabbit secondary antibody labeled with Alexa Fluor 488 at room temperature for 1 h. With the use of a fluorescence microscope (Olympus, Tokyo, Japan), signals were detected, and images were captured and analyzed using cellSens image analysis software (Olympus)

ISH

A locked nucleic acid miR-93-3p probe with a digoxigenin (DIG) label (Exiqon) (5′-DIG-CGGGAAGTGCTAGCTCAGCAGT-DIG-3′) and a scrambled miRNA control probe (5′-GTGTAACACGTCTA TACGCCCA-3′) was used for ISH. Paraffin sections with 5 μm thickness were digested with proteinase K (0.005%; 30 min at 37°C), followed by overnight incubation with freshly labeled probes at 55°C. *In situ* signal was detected by peroxidase-labeled antibody and visualized with diaminobenzidine (DAB).

qRT-PCR

TRIzol reagent (Invitrogen) was used to isolate RNA from tissue and cells, according to the instructions from the manufacturer. cDNA synthesis from RNA was performed using HiScript RT (RNase H; GeneCopoeia, USA). The ABI PRISM 7500 Sequence Detection System (Applied Biosystems, Foster City, CA, USA), with a SYBR Green Master Mix (Vazyme, Nanjing, China), was used for the qPCR. U6 and glyceraldehyde 3-phosphate dehydrogenase (GAPDH) were used for normalization, respectively. Primer sequences for qRT-PCR are displayed in Table S1.

Plasmid construction

Two scrambled miRNAs were used as negative controls (pre-miR-Ctrl for pre-miR-93-3p and anti-miR-Ctrl for anti-miR-93-3p, respectively), which were purchased from GeneChem (Shanghai, China) and used for the overexpression and knockdown of miR-93-3p, pre-miR-93-3p, and the anti-miR-93-3p.The pre-miR-93-3p and anti-miR-93-3p were transfected into HaCaT cells using the Lipofectamine RNAiMAX reagent (Invitrogen).

To knock down ZFP36L1, the shRNA and a scrambled negative control shRNA were manufactured chemically at GeneChem (Shanghai, China), and shRNA sequences were synthesized and cloned into recombinant shRNA expression vectors. To HEK293T cells, lentiviral plasmid DNA pSicoR (10 mg) and each of the packaging plasmid DNAs (5 mg each) (pMDLg/pRRE, pRSV-Rev, and pMD2.G) were added to allow production of the virus. Cells that were infected were selected using 4 μg/mL puromycin (Invitrogen) for 2 weeks, and stable-transfected cell lines were generated. To overexpress ZFP36L1, the ZFP36L1 coding sequences (CDSs) were ligated into the pcDNA3.1 vector (Invitrogen, Carlsbad, CA, USA) and were transfected into HaCaT cells.

Synthesis of shZFX and negative control shRNA lentivirus vectors (GeneChem, Shanghai, China) knocks down ZFX and infection in HaCaT cells. To overexpress ZFX, cDNA amplification of the human ZFX fragment was performed by PCR and cloned into the GV143 expression vector (GeneChem, Shanghai, China) and was transfected into HaCaT cells.

EdU assay

BeyoClick EdU-488 cell proliferation assay kit (Beyotime, Shanghai, China) was used to test cell proliferation according to the manufacturer's protocol. An inverted fluorescence microscope was used to capture images (Olympus, Tokyo, Japan). Green fluorescence indicated positive cells, whereas Hoechst-stained cells were stained with blue fluorescence.

Cell-cycle analysis

Cell-cycle analysis was measured with the Cell Cycle Kit (Invitrogen) according to the manufacturer's instructions. Adherent cells were

harvested by trypsinization and fixed in methanol. Cells were stained with 500 μL of 30 μg/mL propidium iodide (PI) (Sigma) containing 100 μg/mL RNase (Sigma) and 5 μg/mL Triton X-100 (Sigma). Flow cytometry was performed on FACSCalibur (BD Biosciences, Heidelberg, Germany).

Clone-formation assay

The transfected HaCaT cells were seeded on six-well plates at a density of 500 cells/well. After 14 days, cells were fixed with 4% paraformaldehyde for 15 min and washed with PBS; the cells were stained with 0.1% crystal violet for 10 min.

Scratch assay

HaCaT cells were seeded in six-well plates and grown overnight to confluency. Sterile, 200 μL pipette tips were used to create the wound by scratching on the cell monolayers. In order to inhibit proliferation, cells were incubated with mitomycin C (4 μg/mL). After washing three times, cells were incubated at 37°C, and images were taken using an inverted microscope after 24 h. Closure of the wound was assessed based on wound area at 24 h relative to the original size.

Transwell migration assay

Migration assay of HaCaT cells was performed with the aid of 24-well Transwell chambers with inserts of 8 μm pore size (Chemicon, Temecula, CA, USA). Totally, 2×10^4 cells/well in 100 μL serum-free medium were seeded onto the top chamber, and 600 μL of 10% FBS serum medium was added to the bottom chamber as a chemoattractant. After 24 h of incubation using 4% paraformaldehyde, the cells were fixed and subsequently stained with crystal violet. Cells that migrated were assessed in five random fields at 200× magnification using a microscope (Nikon, Tokyo, Japan).

Luciferase reporter assays

The ZFP36L1 3′ UTRs were amplified and cloned into the XbaI site of the pGL3 vector (Promega, Madison, WI, USA) downstream of the luciferase gene to generate the pGL3-ZFP36L1-3′ UTR plasmids. With the use of a QuikChange XL Site-Directed Mutagenesis Kit (Stratagene, Lo Jolla, CA, USA), we generated mutations at the predicted target site of miR-93-3p, as per the manufacturer's instructions. The mutants were named Mut 1 (single mutant), Mut 2 (single mutant), and Mut all (double mutant). 293 cells were cotransfected with pre-miR-93-3p or pre-miR-control (20 nM) plasmids with FuGENE HD transfection reagent (Promega, Madison, WI, USA). After 48 h, we analyzed luciferase activity using the Dual-Luciferase Reporter Assay System (Promega) and normalized to Renilla luciferase.

Western blot assays

HaCaT cells were lysed in radioimmunoprecipitation assay (RIPA) buffer containing protease inhibitors, and protein concentration was determined using the bicinchoninic acid (BCA) method (Pierce, Rockford, IL, USA). Samples (20 μg each) were separated on 10% SDS-PAGE gels and transferred to polyvinylidene fluoride (PVDF) membranes (Millipore, Bedford, MA, USA). Then, membranes were incubated with the following antibodies: rabbit polyclonal anti-ZFP36L1 (Abcam; ab79191, 1:1,000), rabbit polyclonal anti-ZFX (Sigma; SAB2105426, 1:1,000), and rabbit polyclonal anti-GAPDH (Abcam; ab9485, 1:1,000). The membranes were then washed with PBS and incubated with goat anti-rabbit (Abcam; ab6721, 1:10,000) secondary antibodies conjugated to horseradish peroxidase (HRP). We used enhanced chemiluminescence reaction (ECL) to visualize bands (Immunoblot, 23225; Millipore, Billerica, MA, USA). The protein bands were quantified by densitometric analysis using ImageJ.

PCR amplification of the 3′ UTR elements

For the amplification of the 3′ UTR fragments of *ZFX*, we used forward primer 5′-ACGTTTGTAGAGATATTGGCCTTG-3′ and reverse primers UTR1: (2.691 kb) 5′-TCACTTGACCAAACCCTTAAATACC-3′, UTR2: (2.208 kb) 5′-ACACCTGCCTAAAGCACTTGG-3′, UTR3: (1.035 kb) 5′-GCATGACTTACAAAATGCTCTCTCA-3′, UTR4: (552 bp) 5′-ACTTTCACTGTCAAGTGGTCT-3′, UTR5: (345 bp) 5′-AGTACCATCAAGGTAAGCAAGGT-3′, and UTR6: (138 bp) 5′-TAGCATGTTGCCAGTTTTCCCT-3′.

RNA immunoprecipitations

Whole-cell lysates were prepared from confluent HaCaT cells. With the use of equal amounts of lysates (100–300 μg), monoclonal antibodies against *ZFP36L1* or isotype control immunoglobulin G (IgG) were precoated onto protein-A Sepharose beads, followed by extensive washing. Lysates were preabsorbed with 30 μg of IgG. We performed individual pulldowns at 4°C. Then, we amplified 2 μg of recovered RNA per immunoprecipitation and generated cDNA, and qPCR was performed to measure target transcript enrichment.

Site-directed mutagenesis of the ZFX 3′ UTR

The QuikChange II-E Site-Directed Mutagenesis Kit (Stratagene) was used to induce mutation(s) of ARE based on the manufacturer's instructions. Further, for every mutation, the core pentamer AUUUA (ATTTA in the DNA sequence) was mutated to AGGUA (AGGTA in the DNA).

Statistical analysis

GraphPad Prism was used to perform statistical analyses (GraphPad, San Diego, CA, USA). The data are presented as the mean ± SE. A Student's t test was used to compare differences between the two groups, and one-way ANOVA was used to compare differences among multiple groups. The data are representative of at least three separate experiments conducted in triplicate. p values <0.05 indicate statistical significance.

SUPPLEMENTAL INFORMATION

Supplemental Information can be found online at https://doi.org/10.1016/j.omtn.2020.11.017.

ACKNOWLEDGMENTS

This work was financially supported by the National Nature Science Foundation of China (number 81971848).

AUTHOR CONTRIBUTIONS

X.F. and S.Z. performed most experiments and analyzed data. W.C. analyzed data and wrote the manuscript. J.G. conceived the project, performed experiments, analyzed data, and wrote the manuscript. All authors revised and approved the manuscript.

DECLARATION OF INTERESTS

The authors declare no competing interests.

REFERENCES

1. Reinke, J.M., and Sorg, H. (2012). Wound repair and regeneration. Eur. Surg. Res. *49*, 35–43.
2. Gosain, A., and DiPietro, L.A. (2004). Aging and wound healing. World J. Surg. *28*, 321–326.
3. Zhou, T., Wang, N., Xue, Y., Ding, T., Liu, X., Mo, X., and Sun, J. (2016). Electrospun tilapia collagen nanofibers accelerating wound healing via inducing keratinocytes proliferation and differentiation. Colloids Surf. B Biointerfaces *143*, 415–422.
4. Pastar, I., Stojadinovic, O., Yin, N.C., Ramirez, H., Nusbaum, A.G., Sawaya, A., Patel, S.B., Khalid, L., Isseroff, R.R., and Tomic-Canic, M. (2014). Epithelialization in Wound Healing: A Comprehensive Review. Adv. Wound Care (New Rochelle) *3*, 445–464.
5. Grinnell, F. (1992). Wound repair, keratinocyte activation and integrin modulation. J. Cell Sci. *101*, 1–5.
6. Koivisto, L., Heino, J., Häkkinen, L., and Larjava, H. (2014). Integrins in Wound Healing. Adv. Wound Care (New Rochelle) *3*, 762–783.
7. Krampert, M., Bloch, W., Sasaki, T., Bugnon, P., Rülicke, T., Wolf, E., Aumailley, M., Parks, W.C., and Werner, S. (2004). Activities of the matrix metalloproteinase stromelysin-2 (MMP-10) in matrix degradation and keratinocyte organization in wounded skin. Mol. Biol. Cell *15*, 5242–5254.
8. Le, M., Naridze, R., Morrison, J., Biggs, L.C., Rhea, L., Schutte, B.C., Kaartinen, V., and Dunnwald, M. (2012). Transforming growth factor Beta 3 is required for excisional wound repair in vivo. PLoS ONE *7*, e48040.
9. Werner, S., and Grose, R. (2003). Regulation of wound healing by growth factors and cytokines. Physiol. Rev. *83*, 835–870.
10. Ambros, V., Lee, R.C., Lavanway, A., Williams, P.T., and Jewell, D. (2003). MicroRNAs and other tiny endogenous RNAs in C. elegans. Curr. Biol. *13*, 807–818.
11. Li, D., Wang, A., Liu, X., Meisgen, F., Grünler, J., Botusan, I.R., Narayanan, S., Erikci, E., Li, X., Blomqvist, L., et al. (2015). MicroRNA-132 enhances transition from inflammation to proliferation during wound healing. J. Clin. Invest. *125*, 3008–3026.
12. Li, D., Li, X.I., Wang, A., Meisgen, F., Pivarcsi, A., Sonkoly, E., Ståhle, M., and Landén, N.X. (2015). MicroRNA-31 Promotes Skin Wound Healing by Enhancing Keratinocyte Proliferation and Migration. J. Invest. Dermatol. *135*, 1676–1685.
13. Viticchiè, G., Lena, A.M., Cianfarani, F., Odorisio, T., Annicchiarico-Petruzzelli, M., Melino, G., and Candi, E. (2012). MicroRNA-203 contributes to skin re-epithelialization. Cell Death Dis. *3*, e435.
14. Wu, P., Cao, Y., Zhao, R., and Wang, Y. (2019). miR-96-5p regulates wound healing by targeting BNIP3/FAK pathway. J. Cell. Biochem. *120*, 12904–12911.
15. Galloway, A., Saveliev, A., Łukasiak, S., Hodson, D.J., Bolland, D., Balmanno, K., Ahlfors, H., Monzón-Casanova, E., Mannurita, S.C., Bell, L.S., et al. (2016). RNA-binding proteins ZFP36L1 and ZFP36L2 promote cell quiescence. Science *352*, 453–459.
16. Suk, F.M., Chang, C.C., Lin, R.J., Lin, S.Y., Liu, S.C., Jau, C.F., and Liang, Y.C. (2018). ZFP36L1 and ZFP36L2 inhibit cell proliferation in a cyclin D-dependent and p53-independent manner. Sci. Rep. *8*, 2742.
17. Guo, X., Piao, H., Zhang, Y., Sun, P., and Yao, B. (2020). Overexpression of microRNA-129-5p in glioblastoma inhibits cell proliferation, migration, and colony-forming ability by targeting ZFP36L1. Bosn. J. Basic Med. Sci. *20*, 459–470.
18. Zekavati, A., Nasir, A., Alcaraz, A., Aldrovandi, M., Marsh, P., Norton, J.D., and Murphy, J.J. (2014). Post-transcriptional regulation of BCL2 mRNA by the RNA-binding protein ZFP36L1 in malignant B cells. PLoS ONE *9*, e102625.
19. Wang, C., Fu, S.Y., Wang, M.D., Yu, W.B., Cui, Q.S., Wang, H.R., Huang, H., Dong, W., Zhang, W.W., Li, P.P., et al. (2017). Zinc finger protein X-linked promotes expansion of EpCAM^{+} cancer stem-like cells in hepatocellular carcinoma. Mol. Oncol. *11*, 455–469.
20. Kim, B.K., Yoo, H.I., Choi, K., and Yoon, S.K. (2015). miR-330-5p inhibits proliferation and migration of keratinocytes by targeting Pdia3 expression. FEBS J. *282*, 4692–4702.
21. Yu, N., Yang, Y., Li, X., Zhang, M., Huang, J., Wang, X., and Long, X. (2016). MiR-26a inhibits proliferation and migration of HaCaT keratinocytes through regulating PTEN expression. Gene *594*, 117–124.
22. Chang, L., Liang, J., Xia, X., and Chen, X. (2019). miRNA-126 enhances viability, colony formation, and migration of keratinocytes HaCaT cells by regulating PI3 K/AKT signaling pathway. Cell Biol. Int. *43*, 182–191.
23. Wang, L., Yang, G., Zhu, X., Wang, Z., Wang, H., Bai, Y., Sun, P., Peng, L., Wei, W., Chen, G., et al. (2017). miR-93-3p inhibition suppresses clear cell renal cell carcinoma proliferation, metastasis and invasion. Oncotarget *8*, 82824–82834.
24. Li, Y.J., Yang, Z., Wang, Y.Y., and Wang, Y. (2019). Long noncoding RNA ZNF667-AS1 reduces tumor invasion and metastasis in cervical cancer by counteracting microRNA-93-3p-dependent PEG3 downregulation. Mol. Oncol. *13*, 2375–2392.
25. Xuan, P., Dong, Y., Guo, Y., Zhang, T., and Liu, Y. (2018). Dual Convolutional Neural Network Based Method for Predicting Disease-Related miRNAs. Int. J. Mol. Sci. *19*, 3732.
26. Hacker, C., Valchanova, R., Adams, S., and Munz, B. (2010). ZFP36L1 is regulated by growth factors and cytokines in keratinocytes and influences their VEGF production. Growth Factors *28*, 178–190.
27. Zindy, P.J., L'Helgoualc'h, A., Bonnier, D., Le Béchec, A., Bourd-Boitin, K., Zhang, C.X., Musso, O., Glaise, D., Troadec, M.B., Loréal, O., et al. (2006). Upregulation of the tumor suppressor gene menin in hepatocellular carcinomas and its significance in fibrogenesis. Hepatology *44*, 1296–1307.
28. Planel, S., Salomon, A., Jalinot, P., Feige, J.J., and Cherradi, N. (2010). A novel concept in antiangiogenic and antitumoral therapy: multitarget destabilization of short-lived mRNAs by the zinc finger protein ZFP36L1. Oncogene *29*, 5989–6003.
29. Loh, X.Y., Sun, Q.Y., Ding, L.W., Mayakonda, A., Venkatachalam, N., Yeo, M.S., Silva, T.C., Xiao, J.F., Doan, N.B., Said, J.W., et al. (2020). RNA-Binding Protein *ZFP36L1* Suppresses Hypoxia and Cell-Cycle Signaling. Cancer Res. *80*, 219–233.
30. Son, Y.O., Kim, H.E., Choi, W.S., Chun, C.H., and Chun, J.S. (2019). RNA-binding protein ZFP36L1 regulates osteoarthritis by modulating members of the heat shock protein 70 family. Nat. Commun. *10*, 77.
31. Li, H., Yao, G., Zhai, J., Hu, D., and Fan, Y. (2019). LncRNA FTX Promotes Proliferation and Invasion of Gastric Cancer via miR-144/ZFX Axis. OncoTargets Ther. *12*, 11701–11713.
32. Bao, H., Li, X., Li, H., Xing, H., Xu, B., Zhang, X., and Liu, Z. (2017). MicroRNA-144 inhibits hepatocellular carcinoma cell proliferation, invasion and migration by targeting ZFX. J. Biosci. *42*, 103–111.
33. Kota, J., Chivukula, R.R., O'Donnell, K.A., Wentzel, E.A., Montgomery, C.L., Hwang, H.W., Chang, T.C., Vivekanandan, P., Torbenson, M., Clark, K.R., et al. (2009). Therapeutic microRNA delivery suppresses tumorigenesis in a murine liver cancer model. Cell *137*, 1005–1017.
34. Bonci, D., Coppola, V., Musumeci, M., Addario, A., Giuffrida, R., Memeo, L., D'Urso, L., Pagliuca, A., Biffoni, M., Labbaye, C., et al. (2008). The miR-15a-miR-16-1 cluster controls prostate cancer by targeting multiple oncogenic activities. Nat. Med. *14*, 1271–1277.
35. Uchino, K., Takeshita, F., Takahashi, R.U., Kosaka, N., Fujiwara, K., Naruoka, H., Sonoke, S., Yano, J., Sasaki, H., Nozawa, S., et al. (2013). Therapeutic effects of microRNA-582-5p and -3p on the inhibition of bladder cancer progression. Mol. Ther. *21*, 610–619.